*Journal of Applied Electrochemistry* **30**: 1377–1387, 2000.



# Mathematical model of the PEMFC†

K. DANNENBERG[1], P. EKDUNGE[2] and G. LINDBERGH[1]
[1]*Department of Chemical Engineering and Technology, Applied Electrochemistry, Royal Institute of Technology, SE-100 44 Stockholm, Sweden*
[2]*Volvo Technical Development, Chalmers teknikpark, SE-412 88 Göteborg, Sweden*

Received 31 July 1999; accepted in revised form 18 April 2000

*Key words:* heat transfer, mathematical model, PEMFC, proton exchange membrane fuel cell, water management

**Abstract**

A two-dimensional along-the-channel mass and heat transfer model for a proton exchange membrane fuel cell (PEMFC) is described. The model is used for calculation of cell performance (i.e., cell voltage against current density), ohmic resistance and water profile in the membrane, current distribution and variation of temperature along the gas channels. The following fuel cell regions are considered: gas channels, electrode backings and active layers at the anode and cathode side, and a proton exchange membrane. The model includes mass transfer in the gas channels and electrode gas backings, water transport in the membrane, electrode kinetics and heat transfer. Temperature in the cell is assumed to vary only along the gas channels, which means that it is the same at the anode and cathode and in the solid phase at a specified value of the channel coordinate. Electrode kinetics are considered only at the cathode, where major losses occur, whereas the anode potential is assumed to be equal to its equilibrium value. An agglomerate approach is used for the description of the active layer of the cathode. Simulations are carried out for different humidities of inlet gases, several different stoichiometric amounts of reactants and cooling media (air, water) with different heat transfer coefficients. Analysis of the results showed that the best performance of the PEMFC was obtained for well-humidified gases at conditions close to isothermal and at a stoichiometry of gases only somewhat higher than that corresponding to complete reactant consumption.

## List of symbols

| | |
|---|---|
| $a$ | water vapour activity |
| $a_{\mathrm{aggl}}$ | active area of the agglomerate ($\mathrm{cm}^2$) |
| $c_{\mathrm{m}}$ | water concentration in the membrane ($\mathrm{mol\ cm}^{-3}$) |
| $c_{\mathrm{p},i}$ | heat capacity of gas $i$ ($\mathrm{J\ mol}^{-1}\ ^{\circ}\mathrm{C}^{-1}$) |
| $D_{ij}$ | binary diffusion coefficient of the gas mixture of gases $i$ and $j$ ($\mathrm{cm}^2\ \mathrm{s}^{-1}$) |
| $D_{\lambda}$ | diffusion coefficient of water in the membrane ($\mathrm{cm}^2\ \mathrm{s}^{-1}$) |
| $E$ | effectiveness factor |
| $E_{\mathrm{oc}}$ | open circuit voltage of the fuel cell (V) |
| $E_{\mathrm{cell}}$ | fuel cell voltage (V) |
| $F$ | faradaic constant (96 487 C $\mathrm{mol}^{-1}$) |
| $h$ | channel width (cm) |
| $H$ | enthalpy ($\mathrm{J\ mol}^{-1}$) |
| $i_{\mathrm{loc}}$ | geometric current density in the ionomer phase of the active layer ($\mathrm{A\ cm}^{-2}$) |
| $I$ | local geometric current density ($\mathrm{A\ cm}^{-2}$) |
| $I_{\mathrm{avg}}$ | average current density ($\mathrm{A\ cm}^{-2}$) |
| $k$ | kinetic constant ($\mathrm{s}^{-1}$) |
| $k_{\mathrm{eff}}$ | effective conductivity in the active layer ($\mathrm{S\ cm}^{-1}$) |
| $L$ | length of the gas channel (cm) |
| $M_i$ | molar flow of species $i$ ($\mathrm{mol\ s}^{-1}$) |
| $M_{\mathrm{m}}$ | equivalent weight of the membrane ($\mathrm{g\ mol}^{-1}$) |
| $n_{\mathrm{d}}$ | electroosmotic drag coefficient (number of $H_2O$ molecules carried per proton) |
| $N_i$ | $y$-component molar flux of species $i$ ($\mathrm{mol\ cm}^{-2}\ \mathrm{s}^{-1}$) |
| $P$ | pressure (atm) |
| $P_{\mathrm{perm}}(O_2)$ | oxygen permeability in the active layer ($\mathrm{mol\ cm}^{-1}\ \mathrm{s}^{-1}$) |
| $q$ | overall heat transfer coefficient ($\mathrm{W\ cm}^{-2}\ ^{\circ}\mathrm{C}^{-1}$) |
| $R$ | universal gas constant (8.3143 $\mathrm{J\ mol}^{-1}\ \mathrm{K}^{-1}$) |
| $R_{\mathrm{m}}$ | membrane resistance ($\Omega\ \mathrm{cm}^2$) |
| $T$ | local temperature in the fuel cell (°C) |
| $T_{\mathrm{coolant}}$ | coolant temperature (°C) |
| $T_{\mathrm{hum}}$ | humidification temperature of reactant gases (°C) |
| $T_{\mathrm{in}}$ | inlet temperature of anode and cathode gases (°C) |
| $x_i$ | $y$-component mole fraction of species $i$ in the gas backing |

† Dedicated to the memory of Daniel Simonsson

*Greek letters*

| | |
|---|---|
| $\alpha$ | net water flux per molar flux of $H_2$ |
| $\delta$ | thickness of the electrolyte film surrounding agglomerates (cm) |
| $\eta$ | electrode overpotential (V) |
| $\lambda$ | water content in the membrane, moles of water per mole of sulphonic groups |
| $v$ | ratio between the inlet reactant flow and the flow consumed in the fuel cell reaction at average current density $I_{avg} = 1$ A cm$^2$ |
| $\rho_m$ | density of a dry membrane (g cm$^{-3}$) |
| $\sigma_m$ | membrane conductivity (S cm$^{-1}$) |

*Subscripts*

| | |
|---|---|
| a | anode |
| c | cathode |

## 1. Introduction

Proton exchange membrane fuel cells (PEMFC) are particularly suitable for traction applications, due to their high power density, simple and safe construction and fast start-up, even at low temperatures. Nevertheless, for the commercial introduction of the PEMFC as a power source for traction applications or a small-scale power plant, it remains to reduce its cost and to improve its performance and efficiency. This problem can be approached using mathematical models which are useful tools for analysis and optimization of fuel cell performance and also for heat and water management. By this means a simulation of the performance of the whole fuel cell system at different temperatures, humidities, gas compositions and many other parameters can be performed. The results can be used for optimization of various properties of the PEMFC, thus minimizing the time necessary for large amounts of experimental studies.

A two-dimensional mathematical model is preferable for water and heat management analysis, as temperature and water content in the cell normally varies along the gas channels depending on the design of the fuel cell and cooling system. In a one-dimensional model, transport of the reactants is usually considered only into or out of the membrane electrode assembly, and the cell temperature is assumed to be constant. Several such one- and two-dimensional models of a single PEMFC have been developed [1–5].

One-dimensional PEMFC models were developed in the early 1990s by Bernardi et al. [1] and Springer et al. [2]. In the model by Bernardi, the authors concentrated their study on a fully hydrated membrane electrolyte, whereas more detailed description of the water transport in the membrane by means of water drag and diffusion processes at different humidification conditions was given by Springer. Both models were isothermal and mass transport was treated only into or out of the membrane electrode assembly neglecting concentration variations along the gas channels.

Two-dimensional models studying different aspects of the water and heat management have been developed by Fuller et al. [3] and Nguyen et al. [4]. In Fuller's model, concentrated solution theory is used for description of the membrane, and Butler–Volmer kinetics is applied to electron transfer reactions. Nguyen's model describes the membrane electrolyte similarly to Springer's one-dimensional model [2], however, only anode side water content is used for calculation of the parameters, which depend on the membrane water content, neglecting water profile across the membrane. Using this assumption, the values of membrane conductivity can be underestimated, leading to unreasonably high ohmic losses in the membrane. Both Fuller and Nguyen consider coflow pattern when discussing gas channels and heat exchangers. Recently, an improved model was published by Yi and Nguyen which compares different fuel cell designs with coflow and counterflow heat exchangers [5].

Responding to an increasing interest in larger fuel cell systems, a number of mathematical models for the fuel cell stacks have appeared during last few years [6–12]. The full-scale fuel cell systems possess rather complex design of hardware (flow fields, heat exchangers etc.), therefore transport processes of the reactants and products in the gas channels and coolant usually require complicated mathematics. To minimize complexity of the mathematical models, a simplified description of the electrochemical kinetics and mass transport in the electrodes and membrane is often used.

The aim of our work was to develop a two-dimensional mass and heat transfer model which included all important characteristics of the membrane, gas backings and electrode active layer. A more detailed description of the water content in the membrane is given, enabling determination of water profiles across the membrane and more accurate calculation of water content depending parameters. In contrast to the majority of two-dimensional models, which describe the active layer as a film of negligible thickness, the present model uses the agglomerate approach, developed by us previously [13]. The mathematical model is used for cell performance analysis at various conditions, such as different humidification temperatures, stoichiometric coefficients and liquid and air cooling systems.

## 2. Description of the model

Several regions are considered in the fuel cell (Figure 1): a proton-exchange membrane, active layers at the anode and cathode and electrode gas backings. Two coordinate axes are chosen: an $x$ axis, with a direction the same as that for the gas channels, that starts at the fuel cell inlet, and a $y$ axis across the membrane electrode assembly that starts at the fuel cell anode inlet.

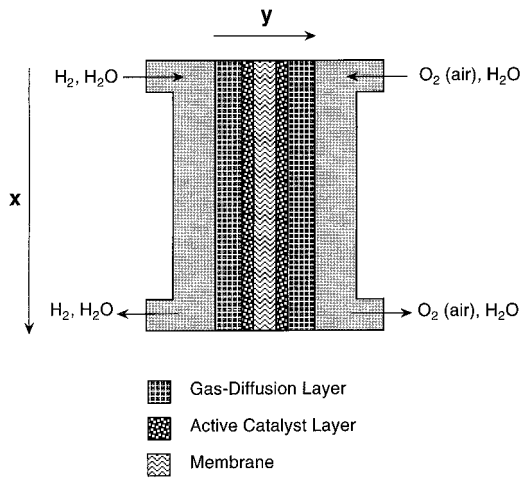


*Fig. 1.* Components of the PEMFC and position of coordinates used in the model.

At the fuel cell inlet, humidified reactant gases are supplied at a given stoichiometry and then react at the active layer to be further transported down to the fuel cell outlet together with the products. The exhaust flow consists of reactants (if stoichiometry is larger than 1) and water vapour, which is supplied by humidified gases and/or produced in the fuel cell reaction.

The flow variations along the gas channels ($x$ direction), due to the flux $N_i$ in the $y$ direction of the reactants or products into or out of the membrane–electrode assembly, are described as follows:

$$\frac{dM_i}{dx} = -hN_i(x) \tag{1}$$

where $i$ is $O_2$, $N_2$ or $H_2O$ vapour at the cathode side and $H_2$ and $H_2O$ vapour at the anode side. Water vapour includes both water produced and water supplied to the fuel cell by humidification of gases. The flux $N_i$ is a function of coordinate $x$ due to the variation of current density in the $x$ direction.

The fluxes of the anode and cathode components are defined as follows:

$$N_{H_2}(x) = \frac{I(x)}{2F} \tag{2}$$

$$N_{O_2}(x) = \frac{I(x)}{4F} \tag{3}$$

$$N_{N_2}(x) = 0 \tag{4}$$

$$N_{H_2O,a}(x) = \frac{\alpha I(x)}{2F} \tag{5}$$

$$N_{H_2O,c}(x) = \frac{(1+\alpha)I(x)}{2F} \tag{6}$$

where $I(x)$ is local geometric current density which varies along the channel due to the variations of temperature, water content, overpotential and conductivity. The value of the current density is assumed to be positive. The flux of nitrogen is set to zero as nitrogen is neither consumed or produced in the fuel cell reaction. The variable $\alpha$ is the net water flux per molar flux of hydrogen molecules (i.e., hydrogen consumed in the fuel cell reaction). The value of $\alpha$ is defined as positive if the net amount of water is transported from the anode to the cathode side, that is, if the amount of water transported from the anode to the cathode side, due to the electroosmotic water drag, is larger than that transported from the cathode back to the anode by diffusion.

Diffusion of the reactants in the porous gas backing is described by the Stefan–Maxwell equation, as similarly used in the one-dimensional model published by Springer et al. [2]:

$$\frac{dx_i}{dy} = RT\sum_j \frac{x_iN_j - x_jN_i}{PD_{ij}} \tag{7}$$

The following equations are obtained for $H_2O$ at the anode, and $O_2$ and $H_2O$ at the cathode:

$$\frac{dx_{H_2O,a}}{dy} = \frac{RTI(x)}{2FP_aD_{H_2O,H_2}}\left[x_{H_2O,a}(1+\alpha) - \alpha\right] \tag{8}$$

$$\frac{dx_{O_2}}{dy} = \frac{RTI(x)}{2FP_c}\left[\frac{x_{O_2}(1+\alpha) + 0.5x_{H_2O,c}}{D_{H_2O,O_2}} + \frac{1 - x_{H_2O,c} - x_{O_2}}{D_{O_2,N_2}}\right] \tag{9}$$

$$\frac{dx_{H_2O,c}}{dy} = \frac{RTI(x)}{2FP_c}\left[\frac{(1 - x_{H_2O,c} - x_{O_2})(1+\alpha)}{D_{H_2O,N_2}} + \frac{0.5x_{H_2O,c} + x_{O_2}(1+\alpha)}{D_{H_2O,O_2}}\right] \tag{10}$$

Binary diffusion coefficients $D_{ij}$ can be calculated by using the Slattery and Bird's approximation is the same way as in [2].

The variable $\alpha$ (net water flux per molar flux of hydrogen) is calculated as follows:

$$\alpha = 2n_d - \frac{2F}{I(x)}D_\lambda\frac{dc_w}{dy} \tag{11}$$

where $n_d$ and $D_\lambda$ are the respective electroosmotic drag and diffusion coefficients of water in the membrane. Both the drag and diffusion coefficients depend upon the water content $\lambda$, amount of water molecules per mole of sulphoic groups in the membrane.

Values of diffusion coefficient were calculated according to Fuller [14]:

$$D_\lambda = 3.5\times10^{-2}\times\frac{\lambda}{14}\exp\left(-\frac{2436}{T+273}\right) \tag{12}$$

The expression for water drag coefficient was adapted from the mathematical model by Springer et al. [2], assuming that the value of the drag coefficient is equal to 3.5 at $\lambda = 20$ for the membrane equilibrated with liquid water.

$$n_d = 3.5 \times \frac{\lambda}{20} \tag{13}$$

The concentration of water can be expressed in terms of water content $\lambda$ and the expression for $\alpha$ can be rewritten:

$$\alpha = 2n_d - \frac{2F}{I(x)} \frac{\rho_m}{M_m} D_\lambda \frac{d\lambda}{dy} \tag{14}$$

where $\rho_m$ and $M_m$ are membrane density and equivalent weight, respectively.

The water content $\lambda$ is a function of water activity and temperature. Usually, the value of $\lambda$ decreases with increasing temperature, if water activity is kept constant. In order to calculate nonisothermal water profiles in the membrane, a data base of water content $\lambda$, covering the whole range of possible activities and temperatures, is needed. Studies reported so far in literature cover only a limited range of temperature values (see Appendix A for more details). To obtain values of $\lambda$ at other temperatures, a numerical interpolation was used. Another important characteristic of water uptake is the fact that it is much higher when the membrane is equilibrated with water in liquid state rather than when it is in contact with water vapour. In the model, water is assumed to be in the vapour form (or water droplets of a zero volume) even at levels above saturation (water activity $a > 1$). To take into account the increase in water uptake, for these activities, the curves for $\lambda$ at different temperatures were extrapolated to $a = 2.5$ (see Appendix A), above which $\lambda$ was assumed to be constant and equal to 20.

Membrane conductivity is calculated by use of an empirical relationship between the conductivity and water content, using data from the paper by Sone et al. [15].

$$\begin{aligned}\sigma = &-0.005\,163\,8 + 0.000\,202\,17\lambda + 0.002\,215\,4\lambda^2 \\ &- 0.000\,277\,2\lambda^3 + 1.4657 \times 10^{-5}\lambda^4 \\ &- 2.7746 \times 10^{-7}\lambda^5\end{aligned} \tag{15}$$

As water content varies through the membrane, a different value of conductivity is obtained at different $y$ values in the membrane (at a fixed coordinate $x$). For each value of $x$, the resistance of the membrane is calculated by integrating:

$$R_m(x) = \int_0^{t_m} \frac{dy}{\sigma(\lambda)} \tag{16}$$

Losses due to the electrode kinetics are only considered for the oxygen reduction reaction. Anode overpotential, when pure hydrogen is used, is small and is neglected in the calculations. The model used for the active layer of the cathode is an agglomerate model developed earlier [13]. In this model, it is assumed that the active layer contains small particles (agglomerates), which consist of platinum, carbon and polymer electrolyte. The agglomerate particles are separated by gas pores which enable the fast transport of oxygen over the whole active layer. Each agglomerate is covered by a thin polymer electrolyte film through which oxygen diffuses into the particles.

Overpotential in the electrolyte phase follows Ohm's law:

$$\frac{\partial \eta}{\partial y} = \frac{i_{loc}}{k_{eff}} \tag{17}$$

The parameter $k_{eff}$ is the effective conductivity of the active layer, and $i_{loc}$ is the local current density in the active layer.

The following expression was obtained for the current density:

$$\frac{\partial i_{loc}}{\partial y} = -4F \left( \frac{1}{\frac{\delta}{a_{aggl} C_{O_2} D_{eff}} + \frac{1}{kE}} \right) \tag{18}$$

The variables $a_{aggl}$ and $\delta$ are the active area of the agglomerate and the thickness of the electrolyte film, surrounding each agglomerate, respectively. Product $C_{O_2} D_{eff}$ is equal to the oxygen permeability (on calculation of permeability, detailed in Appendix B), whilst $k$ and $E$ are the kinetic constant and effectiveness factor, respectively. The kinetic reaction constant was obtained from a simplified Butler–Volmer equation, neglecting the rate of the backwards reaction, and the effectiveness factor was calculated with Thiele's modulus. Detailed description of the agglomerate model as well as parameters used can be found in [13].

The cell voltage is calculated from the membrane resistance, current density and electrode overpotentials, as follows:

$$E_{cell} = E_{oc} - \eta(x) - I(x) R_m(x) \tag{19}$$

Electrode overpotential in the model only includes cathode overpotential as mentioned above.

The average current density for a given cell voltage is calculated by integrating along the whole channel length:

$$I_{avg} = \frac{1}{L} \int_0^L I(x) dx \tag{20}$$

$I(x)$ is a local geometric current density at each point along the channel, and $L$ is the length of the channel.

Temperature of the inlet gases is set to the same value as the fuel cell inlet temperature (70 °C) irrespective of the humidification temperature. It is assumed that the temperature is only a function of the channel coordinate $x$, that is, it is the same for the anode and cathode gases and the solid components of the fuel cell, at a specified

value of coordinate $x$. Variations of temperature along the gas channels are calculated according to the following energy balance equation:

$$dM_i\Delta H_i(T) = \sum M_i(x)c_{p_i}(T)dT + E_{cell}I(x)h\,dx + q(T - T_{coolant})h\,dx \quad (21)$$

where $M_i$ is a molar flow of a component $i$, $\Delta H$ the enthalpy change per mole of gas and $c_p$ the heat capacity of each component. Enthalpy changes at a given temperature and the heat capacities of the gases are calculated as done by Newman et al. [3]. The product $E_{cell}I(x)$ represents the electrical work provided by the system, $I(x)$ is the local geometric current density and $h$ is the width of the channel. The last term in the energy balance represents the heat transfer to the cooling system, and includes the overall heat transfer coefficient $q$ and temperatures of the gases and coolant ($T$ and $T_{coolant}$). The overall heat transfer coefficient includes heat transfer effects both in the coolant and gas flows. Coolant is supplied to both sides of the fuel cell like in a fuel cell stack where cooling plates are placed between each cell. The temperature of the coolant is assumed to be constant along the gas channels, which corresponds to a very large flow rate of coolant (air or water).

The model equations are solved numerically at a given value of cell voltage. A value of the local current density $I(x)$ is initially guessed, and one-dimensional equations for the mass transport into or out of the membrane–electrode assembly and kinetic expressions are solved for the actual value of $x$. On the basis of these results, mass transport along the channel length and temperature variations are calculated. The cell voltage is then calculated and compared with the specified value. If the calculated value disagrees with the specified one, a new value of $I(x)$ is given, by numerical iteration, until both values agree. This procedure is repeated until all the model equations are solved for the whole channel. Finally, the average current density and membrane resistance are calculated.

## 3. Results and discussion

Calculations were performed for various humidification temperatures, different stoichiometric amounts of reactants and several heat transfer coefficients (gas and liquid coolants).

Polarization curves (cell voltage against average current density) and curves showing ohmic resistance as a function of current density were obtained. At constant cell voltage, usually $E_{cell} = 0.6$ V, variations of current density, ohmic resistance, temperature along the gas channels, as well as water profile in the membrane ($\lambda$ as a function of the membrane coordinate $y$ and channel coordinate $x$), were calculated.

### 3.1. *Base case calculations*

To analyse the influence of different parameters on cell performance, a base case (cell and humidification temperatures 70 °C, stoichiometry 2 at $I_{avg} = 1$ A cm$^{-2}$) was chosen. Parameter values used for the base case are shown in Table 1. Pure oxygen and hydrogen at atmospheric pressure were used in all calculations. These were chosen as most of the experimental studies at our laboratory, on one-dimensional small-scale fuel cell, were carried out at similar conditions [13], as well as empirical relationships obtained either from the literature or our own studies were best defined at these conditions. Nafion® 115 membrane was chosen as the electrolyte.

Simulated curves for the base case are given in Figure 2: polarization curve and ohmic resistance in the membrane (a), current density and temperature profiles along the channel coordinate at constant value of $E_{cell} = 0.6$ V (b), membrane resistance variations (c) as well as water profile in the membrane (d).

As mentioned above, the Stefan–Maxwell equation is applied for the description of the gas transport in a porous gas backing. However, preliminary calculations showed that in the case of pure gases, influence of gas transport limitations through the highly porous gas backing was negligible. In order to minimize the time necessary for each simulation, the Stefan–Maxwell equation was omitted, that is, it was assumed that concentrations of gases in the active layer at the membrane–electrode interface are the same as in the gas channels. It should be noted that in the case of air at the cathode or if the anode gas contains other components than pure hydrogen, a transport equation in the gas backing should be used, especially at low stoichiometries.

The polarization curve and ohmic resistance in the membrane shown in Figure 2(a), follow the general trend observed for PEMFC at atmospheric pressure [2, 16, 17]. For current densities higher than 1 A cm$^{-2}$, some mass transport limitations can be observed, which arise from oxygen diffusion through the electrolyte film surrounding the agglomerate particles. Ohmic resistance is fairly constant up to $I_{avg} = 0.8$ A cm$^{-2}$, and then increases somewhat due to the water drag from the anode to the cathode and insufficient back-diffusion. Variations in current density, temperature and ohmic resistance, along the channel coordinate, as

*Table 1.* Parameter values for the base case

| Parameter | Value |
|---|---|
| Pressure of reactant gases, $P$ | 1 atm |
| Stoichiometric coefficient, $\nu$ | 2 |
| Fuel cell inlet temperature, $T_{in}$ | 70 °C |
| Humidification temperatures of $O_2$ and $H_2$, $T_{hum}$ | 70 °C |
| Temperature of the liquid coolant, $T_{coolant}$ | 65 °C |
| Heat transfer coefficient, $q$ | 0.08 W cm$^{-2}$ °C$^{-1}$ |
| Channel length, $L$ | 10 cm |
| Channel width, $h$ | 1 cm |

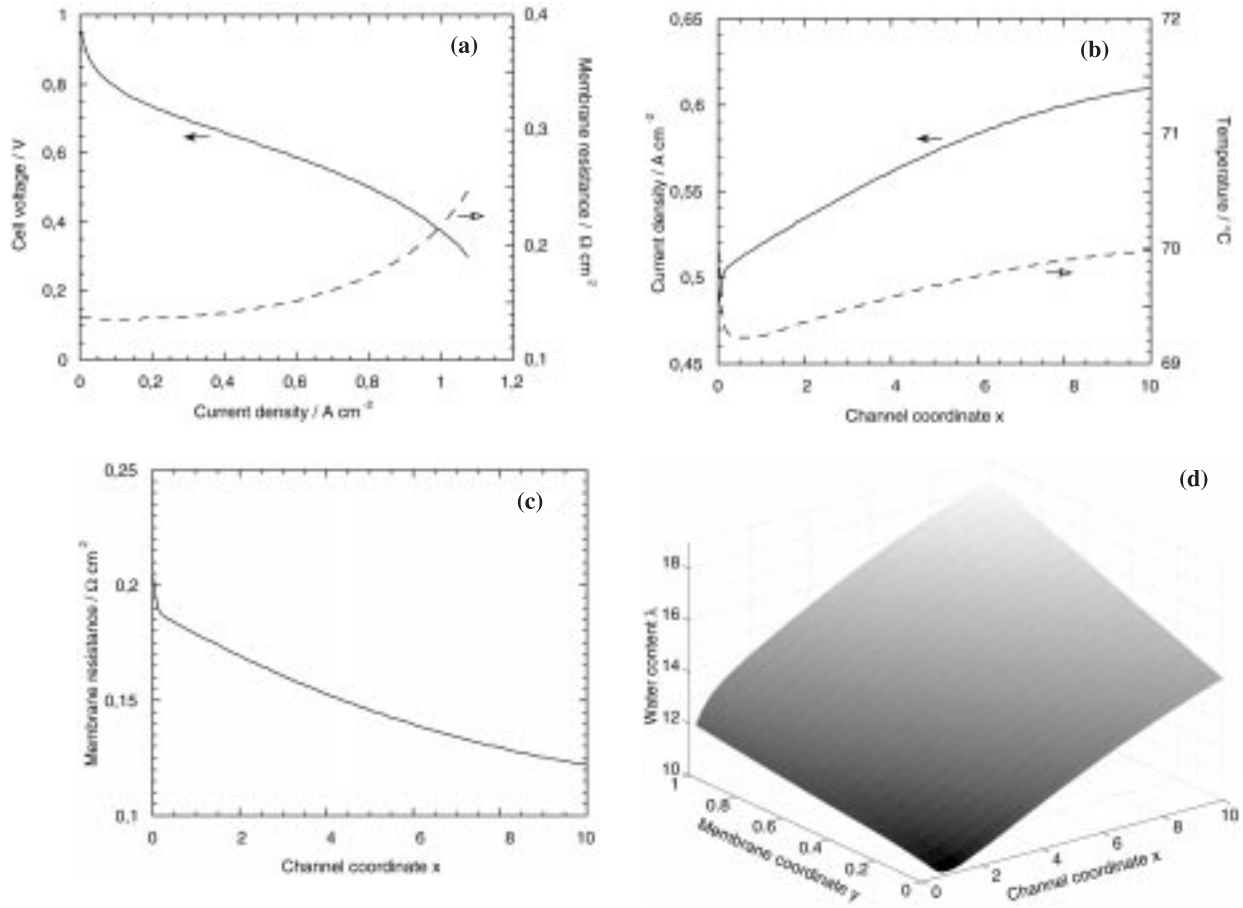


*Fig. 2.* Simulated curves for the base-case: polarization curve, ohmic resistance in the membrane as a function of current density (a), current density and temperature profiles (b), variations of membrane resistance along the gas channels (c), water profile in the membrane (d) at $E_{cell} = 0.6$ V.

well as the water profile, at constant cell voltage, are shown in Figure 2(b)–(d). The cell voltage value of 0.6 V was chosen as a typical PEMFC operation voltage. Figure 2(b) shows current density and temperature variations. Both their values are fairly constant along the gas channel; the current density increases only slightly (resulting in small increases in temperature) due to improved water content in the membrane and lower ohmic resistance close to the cell outlet.

The water content profile for the base case is shown in Figure 2(d). Coordinates (0,0) and (10,0), respectively, correspond to the membrane/electrode interfaces at the anodic side inlet and outlet. In the same way, coordinates (0,1) and (10,1) correspond to the interfaces on the cathodic side. Already at the inlet, the water profile is established across the membrane, that is, the water content at the anode side is lower than that at the cathode side. This is due to the electroosmotic drag of water, from the anode to cathode, and insufficient backdiffusion from the cathode side, where water is produced, to the anode side. Water production at the cathode results in increasing water content in the membrane along the gas channels (coordinate $x$) both at the cathode and anode, and it follows the same shape as the water profile across the membrane (coordinate $y$) at the inlet, that is, water content at the anode is lower than that at the cathode. Even if the increased water production leads to higher water content in the whole membrane, both the water drag coefficient and diffusion coefficient increase linearly with the water content, and the shape of the water profile across the membrane remains unaltered.

In further simulations, discussed below, the influences of various parameters are investigated by varying one parameter at time, maintaining the remaining parameters at the values of the base case, if not otherwise stated.

### 3.2. *Influence of the humidification temperature*

Simulated curves obtained for a constant cell temperature and various humidification temperatures are shown in Figures 3 and 4(a)–(c).

In Figure 3, the cell performance and membrane resistance are compared at a cell inlet temperature of 70 °C and humidification temperatures of 50–80 °C. Cell performance increases remarkably when the humidification temperature is increased from 50 to 60 and 70 °C, due to the higher water content in the membrane at the

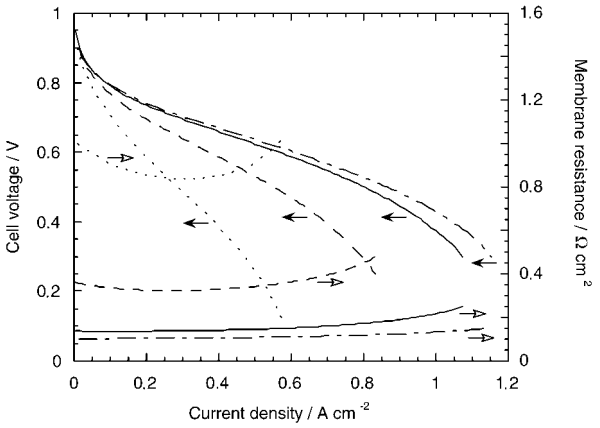


*Fig. 3.* Voltage–current curves and membrane resistance as a function of current density for various humidification temperatures: 50 °C (· · ·), 60 °C (– – –), 70 °C (——) and 80 °C (– · – · –).

higher humidification temperatures (see water profiles in Figure 5) and lower ohmic resistance. A further increase in humidification temperature improves the performance only slightly, as the membrane has almost reached its minimum resistance at the humidification temperature of 70 °C (water activity is larger than one at the cathode side already at the inlet, due to fact that the inlet gases are humidified up to 100% and additional water is produced at the cathode). Another reason why cell performances, at gas humidification temperatures of 70 and 80 °C, are rather similar is the fact that the oversaturation of the reactant gases leads to some depletion of the oxygen at the cathode side. This can be observed in Figure 4a showing the variation of current density along the gas channels. For $T_{hum} = 80$ °C, current density decreases to some extent from the cell inlet to the outlet due to decreased oxygen concentration in the cathode gas, resulting from water production at the cathode and oversaturation of the inlet gas. In contrast, for $T_{hum} = 50$, 60 and 70 °C, current density increases with channel coordinate, due to increased water content in the membrane and lowering of ohmic resistance. This also leads to some temperature increase. The average current densities increase with humidification temperature up to 70 °C, and then remain almost unaltered for the next value of $T_{hum} = 80$ °C for the above reasons. This leads to the conclusion that the values of relative humidity of the inlet gas should not be higher than 100% because of the depletion of oxygen concentration. Another possible reason is the formation of a water film, at the cathode, that is not considered in the present model but would still limit oxygen diffusion.

### 3.3. *Influence of the stoichiometric coefficient*

The influence of the reactant stoichiometry was evaluated for the fuel cell inlet temperature and gas humidification temperature of 70 °C. The stoichiometric coefficients $v$, used in the simulations, were 0.7, 1, 2 and 3. Polarization curves and ohmic resistance at different current densities are shown in Fig. 6. Exam-

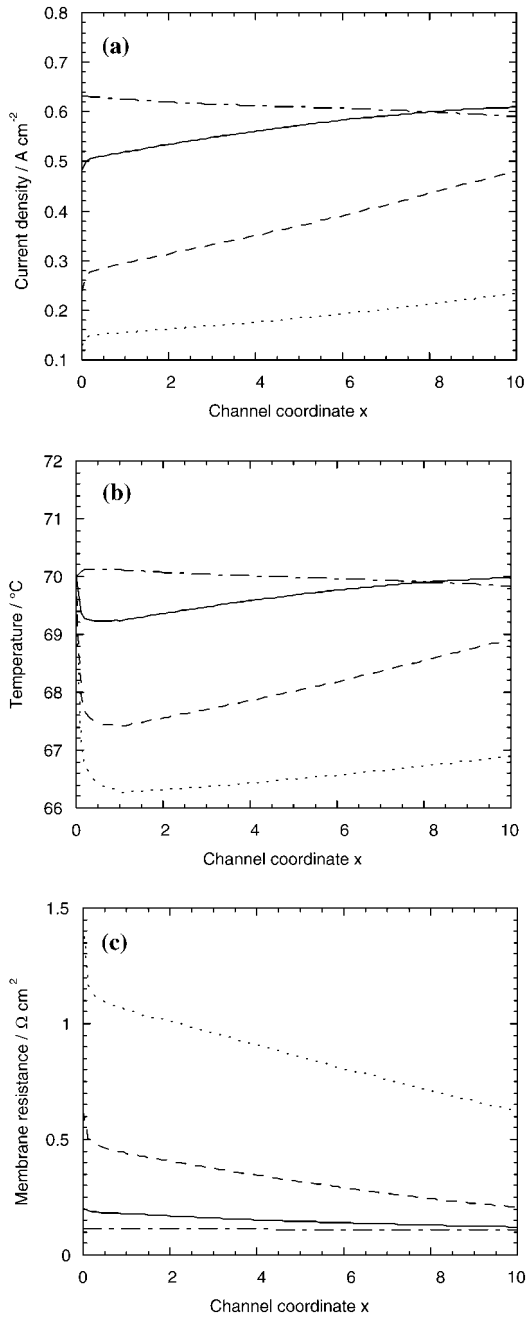


*Fig. 4.* Variations in current density (a), temperature (b) and membrane resistance (c) along the gas channels for various humidification temperatures: 50 °C (· · ·), 60 °C (– – –), 70 °C (——) and 80 °C (– · – · –).

ination of the curves leads to the following observations: (i) cell performance, especially at high current densities, is improved when the stoichiometric coefficient increases from 0.7 to 2 and decreases somewhat when this value is equal to 3, (ii) ohmic resistance increases with an increasing value of the stoichiometric coefficient. The effects of the stoichiometric coefficient on the current density and ohmic resistance can be seen more clearly in Figure 7(a)–(c), from their variations along the gas channels at a constant cell voltage. At low values of $v$, depletion of the reactants can be observed close to the outlet, and this is the reason why current

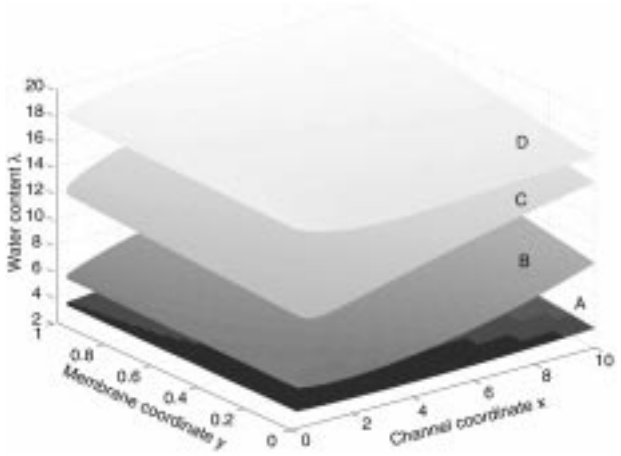


*Fig. 5.* Water profile in the membrane at cell voltage 0.6 V for several humidification temperatures: 50 °C (A), 60 °C (B), 70 °C (C) and 80 °C (D).

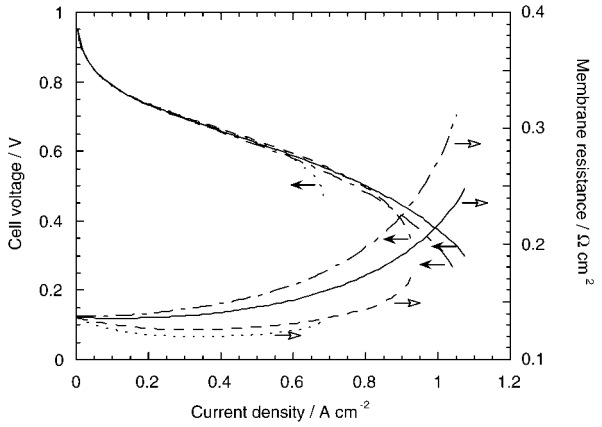


*Fig. 6.* Voltage–current curves and membrane resistance as a function of current density for different stoichiometric amounts of the reactants: $v = 0.7$ (· · ·), $v = 1$ (– – –), $v = 2$ (——), $v = 3$ (– · – · ·).

density decreases at the outlet (Figure 7(a)). On the other hand, high values of the stoichiometric coefficient increase ohmic resistance, due to the fact that the inlet reactant gas is dryer that the outlet gas, because water is formed in the fuel cell reaction. This means that the values of the stoichiometric coefficient have two different effects on the total performance of the fuel cell: (i) at low values of $v$, the cell is well humidified (assuming sufficient humidification of the inlet gases), but current density decreases along the gas channels due to the depletion of the reactants; (ii) at high values of $v$, the amount of reactants is sufficient, but current density decreases due to the higher ohmic resistance, which is caused by the high flow of the inlet gas that has lower humidity than the outlet gas. These two effects compete in the fuel cell, which can be seen from the polarization curves in Figure 6, namely, where the cell performance increased up to a $v$ value of 2 and decreased somewhat for $v = 3$. In this study, the best cell performance was therefore obtained for the stoichiometric coefficient $v = 2$.

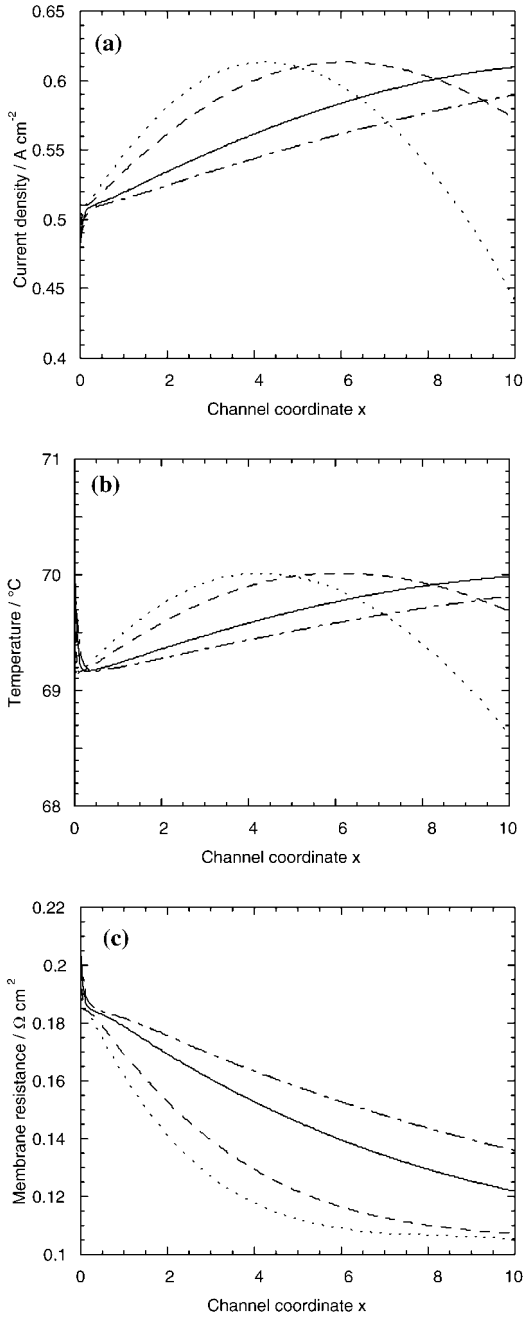


*Fig. 7.* Variations in current density (a), temperature (b) and membrane resistance (c) along the gas channels for various stoichiometric coefficients: $v = 0.7$ (· · ·), $v = 1$ (– – –), $v = 2$ (——), $v = 3$ (– · – · ·).

### 3.4. *Influence of the cooling medium and the heat transfer coefficient*

Heat removal in the fuel cell system is necessary, due to the exothermic character of the cell reaction. It can be performed by using a cooling system operating on air or water, or insuring a large excess of reactant gases. In this paper, the efficiency of air and water coolants is compared and the influence of the value of the heat transfer coefficient is discussed. As the exact values of the heat transfer coefficient were not known, several typical values for air and liquid coolants [18] were used in simulations.

The simulated curves for the fuel cell, operating with air coolant are shown in Figure 8(a)–(c). The value of the heat transfer coefficient $q$ was varied from 0.0070 to 0.0075 W cm$^{-2}$ °C$^{-1}$. Temperature of the air was assumed to be constant and equal to 25 °C. As shown in Figure 8(b), temperature of the fuel cell increases strongly at the inlet, which leads to a lowering of the water content in the membrane, high ohmic resistances and a decreased current density. These effects are more significant for lower values of heat transfer coefficient.

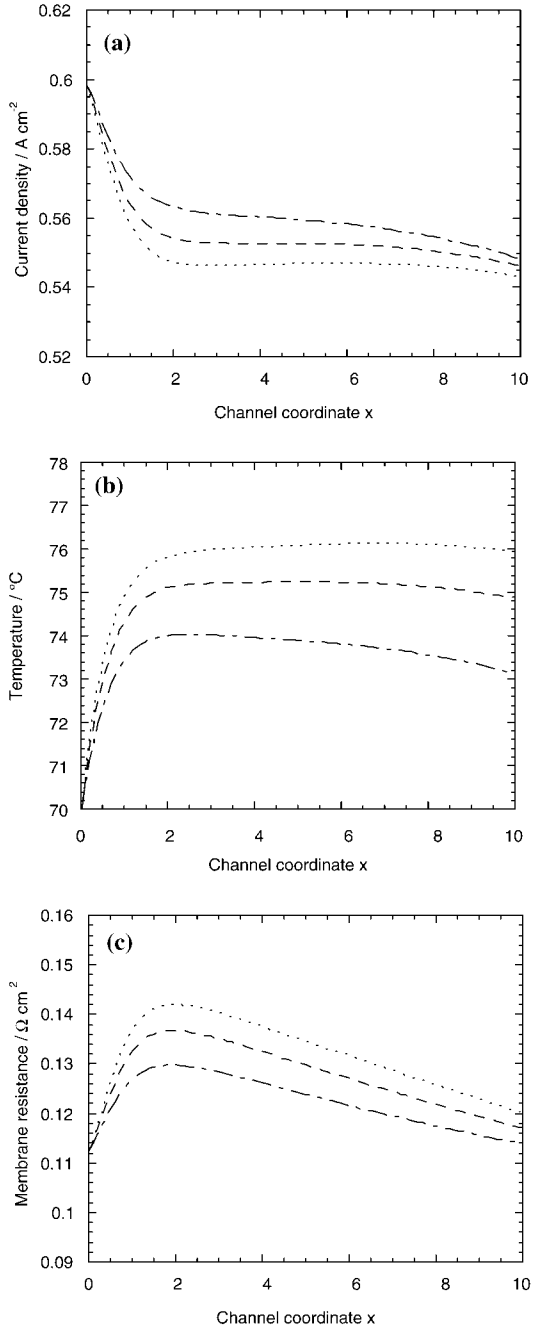


*Fig. 8.* Variations in current density (a), temperature (b) and membrane resistance (c) along the gas channels for several values of heat transfer coefficient (humidification temperature 80 °C, cell inlet temperature 70 °C, gas coolant temperature 25 °C): 0.007 (· · ·), 0.0072 (– – –), 0.0075 W cm$^{-2}$ °C$^{-1}$ (– · – ·).

Results for the water coolant are shown in Figures 9 and 10. Values of the heat transfer coefficient, used in the simulations, were 0.06, 0.07 and 0.08 W cm$^{-2}$ °C$^{-1}$ which are reasonable for a liquid coolant [18]. Variations in the fuel cell temperature, along the gas channels, are almost non-existing in comparison to the case of the air coolant, due to the higher efficiency of the liquid coolant. In the base case of $q = 0.08$ W cm$^{-2}$ °C$^{-1}$ gas channel temperature is very close to that at the inlet. The corresponding water profile in the membrane is shown in Figure 5. Water content is lower at the anode side than at the cathode, but it still increases in the whole membrane in the direction from inlet to outlet. This results in a somewhat improved cell performance, that is, higher current density and lower ohmic resistance (Figures 10(a) and (c)) closer to the cell outlet which was not the case for the air coolant. On the basis of these results, it can be concluded that the best cell performance can be obtained at conditions close to isothermal with efficient cooling. Using liquid coolant, such conditions can be achieved more easily than in the case of air cooling.

## 4. Conclusions

It can be concluded that the best performance of the fuel cell can be obtained at conditions close to isothermal. This is due to the fact that increasing temperature causes drying out of the membrane as both water activity and membrane capability to accumulate water decrease with increasing temperature. A liquid coolant is preferable.

Two competing effects of the stoichiometric coefficient, depending on humidity conditions in the fuel cell, were observed: for well humidified reactant gases increase in stoichiometric coefficient up to certain level (depending on the actual humidity rates of the reactants) eliminates depletion of oxygen and improves cell performance, whereas for dry reactant gases or incompletely humidified (relative humidity <100%) high values of the

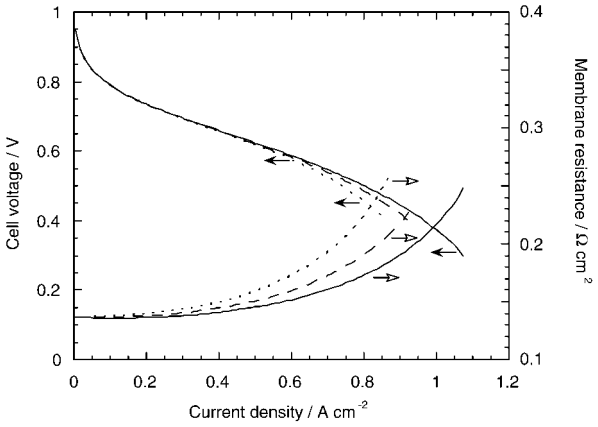


*Fig. 9.* Voltage–current curves and membrane resistance as a function of current density for several heat transfer coefficients (humidification temperature 70 °C, cell inlet temperature 70 °C, liquid coolant temperature 65 °C): 0.006 (· · ·), 0.007 (– – –), 0.008 W cm$^{-2}$ °C$^{-1}$ (– · – ·).

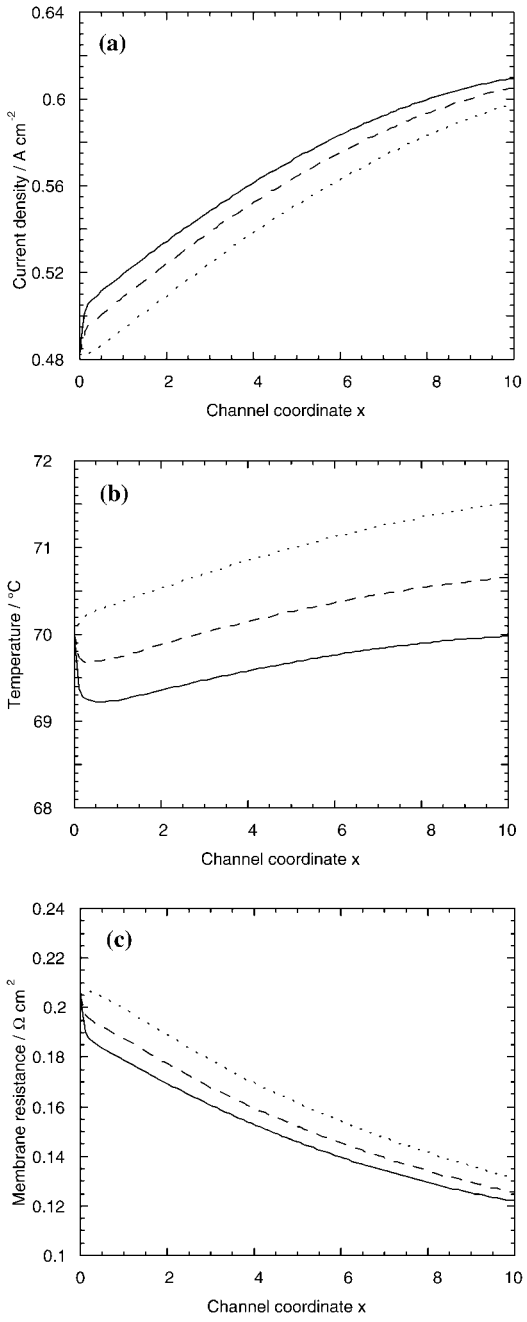


*Fig. 10.* Variations in current density (a), temperature (b) and membrane resistance (c) along the gas channels for various heat-transfer coefficients (cell conditions the same as in Figure 9): 0.006 (· · ·), 0.007 (– – –), 0.008 W cm$^{-2}$ °C$^{-1}$ (——).

stoichiometric coefficient causes drying out of the membrane which results in higher ohmic resistance. The best performance was obtained for a reactant stoichiometry of 2.

Analysis of the influence of the humidification temperatures showed that performance is remarkably improved when the humidification temperature is raised from 50 to 70 °C, and only slightly when this temperature is further increased to 80 °C. This observation may be explained by the fact that increasing humidity of the gases improves the water content in the membrane thus minimizing ohmic losses, whereas if the humidification temperature is too high, depletion in oxygen concentration may occur, especially close to the cell outlet.

In general, the model was found to be useful for analysis of the influence of humidity, stoichiometry of gases and properties of the coolant, on the cell performance, over a wide range of experimental conditions, especially for reactant gases humidified at temperatures close to the fuel cell inlet temperature or lower than this. For simulation of the cell performance, operating with gases humidified at temperatures much higher than that of the fuel cell, or if liquid water is added to gases in the fuel cell, a model describing two-phase water transport would be needed.

## Acknowledgements

Devoting this paper to the memory of Prof. Daniel Simonsson, we would like to express our gratitude to him as one of the initiators of the project. His interest, enthusiasm and contribution to this work was much appreciated. In addition, we would like to acknowledge STEM, the Swedish National Energy Administration, for the financial support of this project.

## References

1. D.M. Bernardi and M.W. Verbrugge, *J. Electrochem. Soc.* **139** (1992) 2477.
2. T.E. Springer, T.A. Zawodzinski and S. Gottesfeld, *J. Electrochem. Soc.* **138** (1991) 2334.
3. T.F. Fuller and J. Newman, *J. Electrochem. Soc.* **140** (1993) 1218.
4. T.V. Nguyen and R. White, *J. Electrochem. Soc.* **140** (1993) 2178.
5. J.S. Yi and T.V. Nguyen, *J. Electrochem. Soc.* **145** (1998) 1149.
6. D. Thirumalai and R. White, *J. Electrochem. Soc.* **144** (1997) 1717.
7. G. Maggio, V. Recupero and C. Mantegazza, *J. Power Sources* **62** (1996) 167.
8. J.C. Amphlet, R.M. Baumert, R.F. Mann, B.A. Peppley, P.R. Roberge and A. Rodriges, *J. Power Sources* **49** (1994) 349.
9. J.C. Amphlett, R.M. Baumert, R.F. Mann, B.A. Peppley, P.R. Roberge and T.J. Harris, *J. Electrochem. Soc.* **142** (1995) 1.
10. J.C. Amphlett, R.M. Baumert, R.F. Mann, B.A. Peppley, P.R. Roberge and T.J. Harris, *J. Electrochem. Soc.* **142** (1995) 9.
11. J.H. Lee, T.R. Lalk and A.J. Appleby, *J. Power Sources* **70** (1998) 258.
12. J.H. Lee and T.R. Lalk, *J. Power Sources* **73** (1998) 229.
13. K. Broka (Dannenberg) and P. Ekdunge, *J. Appl. Electrochem.* **27** (1997) 281.
14. T.F. Fuller, 'Solid Polymer Electrolyte Fuel Cells', PhD thesis, University of California (1995).
15. Y. Sone, P. Ekdunge and D. Simonsson, *J. Electrochem. Soc.* **143** (1996) 1254.
16. E.A. Ticianelli, C.R. Derouin, A. Redondo and S. Srinivasan, *J. Electrochem. Soc.* **135** (1993) 201.
17. J. Kim, S-M. Lee, S. Srinivasan and C.E. Chamberlin, *J. Electrochem. Soc.* **142** (1995) 2670.
18. R.H. Perry and D.W. Green (Eds) 'Perry's Chemical Engineers' Handbook', McGraw-Hill Professional Publishing (1997).
19. T.A. Zawodzinski, Jr., T.E. Springer, J. Davey, R. Jestel, C. Lopez, J. Valerio and S. Gottesfeld, *J. Electrochem. Soc.* **140** (1993) 1981.
20. J.T. Hinatsu, M. Mizuhata and H. Takenaka, *J. Electrochem. Soc.* **141** (1994) 1493.
21. K. Broka (Dannenberg) and P. Ekdunge, *J. Appl. Electrochem.* **27** (1997) 117.

## Appendix A: Calculation of the water content $\lambda$

Through use of the experimental data reported in the literature, empirical relationships between water content and water activity were obtained. Their general form is a polynomial expression:

$$\lambda = k_0 + k_1 a + k_2 a^2 + k_3 a^3 \quad \text{(A1)}$$

Values of the coefficients $k$ are presented in the Table 2. Coefficients for water activities $a \leqslant 1$ at 30 °C were adapted from the papers [2, 19], whereas values for 80 °C were obtained from experimental data by Hinatsu et al. [20]. For water activities $a \geqslant 2.5$, the water content in the membrane was assumed to be constant and equal to 20. For the activity region $1 < a < 2.5$, the water content curves were assumed to follow the same trend as for lower activities, and corresponding polynomial coefficients were obtained by extrapolating the curves to $\lambda = 20$ at $a \geqslant 2.5$. Values of $\lambda$ for other temperatures were obtained by numerical interpolation.

*Table 2.* Coefficients for the calculation of the water content $\lambda$

| Activity, $a$ | Temperature | $k_0$ | $k_1$ | $k_2$ | $k_3$ |
|---|---|---|---|---|---|
| $a \leqslant 1$ | 30 | 0.043 | 17.81 | −39.85 | 36.00 |
| $a \leqslant 1$ | 80 | 0.30 | 10.80 | −16.00 | 14.10 |
| $1 < a < 2.5$ | 30 | −9.1776 | 37.276 | −15.877 | 2.255 |
| $1 < a < 2.5$ | 80 | −30.412 | 61.978 | −25.960 | 3.7008 |
| $a \geqslant 2.5$ | 30 | $\lambda = 20$ | | | |
| | 80 | $\lambda = 20$ | | | |

## Appendix B: Calculation of the oxygen permeability in the active layer

Oxygen permeability in the active layer is calculated on the basis of Henry's law. Solubility constant in the Henry's law's expression was derived from experimental permeability data [21], assuming a constant diffusion coefficient. The following relationship was obtained:

$$P_{\text{perm}}(O_2) = 1.334 \times 10^{-9} P_{O_2} \quad \text{(B1)}$$

Temperature and water content variations in the fuel cell, equipped with an adequate cooling system, are not large, as shown in Figure 2(b) and (d). Influence of these parameters (within the characteristic ranges) on the oxygen permeability values in the active layer was estimated to be small and was not taken into account in the mathematical model.